Profiling and Imaging of Lipids on Brain and Liver Tissue by Matrix-Assisted Laser Desorption/Ionization Mass Spectrometry Using 2-Mercaptobenzothiazole as a Matrix

ARTICLE *in* ANALYTICAL CHEMISTRY · NOVEMBER 2008

Impact Factor: 5.64 · DOI: 10.1021/ac801662n · Source: PubMed

9 AUTHORS, INCLUDING:

Egoitz Astigarraga
IMG Pharma BIotech S.L.
19 PUBLICATIONS **210** CITATIONS
SEE PROFILE

Begona Ochoa
University of the Basque Country, Leioa, S…
113 PUBLICATIONS **1,212** CITATIONS
SEE PROFILE

Rafael Rodriguez-Puertas
Universidad del País Vasco / Euskal Herrik…
46 PUBLICATIONS **856** CITATIONS
SEE PROFILE

José Andrés Fernández
Universidad del País Vasco / Euskal Herrik…
118 PUBLICATIONS **876** CITATIONS
SEE PROFILE

Article

Profiling and Imaging of Lipids on Brain and Liver Tissue by Matrix-Assisted Laser Desorption/Ionization Mass Spectrometry Using 2-Mercaptobenzothiazole as a Matrix

Egoitz Astigarraga, Gabriel Barreda-Go#mez, Laura Lombardero, Olatz Fresnedo, Fernando Castan#o, Mari#a Teresa Giralt, Begon#a Ochoa, Rafael Rodri#guez-Puertas, and Jose# A. Ferna#ndez

Anal. Chem., **2008**, 80 (23), 9105-9114 • Publication Date (Web): 30 October 2008

Anal. Chem. **2008,** *80,* 9105–9114

Profiling and Imaging of Lipids on Brain and Liver Tissue by Matrix-Assisted Laser Desorption/ Ionization Mass Spectrometry Using 2-Mercaptobenzothiazole as a Matrix

Egoitz Astigarraga,[†] Gabriel Barreda-Gómez,[‡] Laura Lombardero,[‡] Olatz Fresnedo,[§] Fernando Castaño,[†] María Teresa Giralt,[‡] Begoña Ochoa,[§] Rafael Rodríguez-Puertas,[‡] and José A. Fernández*[,†]

Department of Chemical Physics, Faculty of Science and Technology, Department of Pharmacology, and Department of Physiology, Faculty of Medicine and Dentistry, University of the Basque Country, B° Sarriena s/n, 48940 Leioa, Spain

2-Mercaptobenzothiazole (MBT) is employed for the first time as a matrix for the analysis of lipids from tissue extracts using matrix-assisted laser desorption/ionization time-of-flight mass spectrometry. We demonstrate that the performance of MBT is superior to that of the matrixes commonly employed for lipids, due to its low vapor pressure, its low acidity, and the formation of small crystals, although because of the strong background at low *m/z*, it precludes detection of species below ~500 Da. This inconvenience can be partly overcome with the formation of Cs adducts. Using a polymer-based dual calibration, a mass accuracy of ~10 ppm in lipid extracts and of ~80 ppm in tissues is achieved. We present spectra from liver and brain lipid extracts where a large amount of lipid species is identified, in both positive and negative ion modes, with high reproducibility. In addition, the above-mentioned special properties of MBT allow its employment for imaging mass spectrometry. In the present work, images of brain and liver tissues showing different lipid species are presented, demonstrating the advantages of the employment of MBT.

In addition to being structural components of the cell membranes that enable spatial segregation of functions and to serving as energy storage, lipids (i.e., lysophospholipids and endocannabinoids) are very specialized in some organs such as the brain where they play a critical role in processes as diverse as neurotransmission, signal transduction, vesicular trafficking, apoptosis, and transcriptional and post-translational regulation.[1] Such a remarkable diversity of functions is due to the thousands of different lipid products that are generated thanks to the complex metabolic pathways that the eukaryotic genome is capable of generating.[2] In the past few years, the mass spectrometry-based techniques have been successfully applied to the identification and characterization of lipids in complex samples[3] or even directly in tissues.[4] In particular, the employment of time-of-flight mass spectrometry (TOFMS), in its different experimental arrangements, offers several advantages when compared with commonly used chromatographic separation-based methodologies. TOFMS is a fast, robust technique, which does not require long and complex preparation or purification protocols. In a single experiment, an enormous amount of information is obtained, in a highly dynamic range (from pmol/μL to mmol/μL). Impurities are generally not a problem as each species usually appears in a different mass channel. In addition, the analysis process is easily automatable and, therefore, transformed into a high-throughput technique. The analysis of lipids by TOFMS can be carried out not only in extracted and purified samples[3,5−9] but also directly in intact tissues, after a simple treatment.[10] Such a strategy eliminates the employment of extraction procedures that may introduce changes in the original lipids' composition.

The development of the so-called imaging mass spectrometry (IMS)[11−14] opened a new field in which new information is obtained in addition to that which is obtained in a normal MS

* To whom correspondence should be addressed. E-mail: josea.fernandez@ehu.es. Phone: +3494 601 5387. Fax: +3494 601 3500.

[†] Department of Chemical Physics.

[‡] Department of Pharmacology.

[§] Department of Physiology.

(1) van Meer, G.; Voelker, D. R.; Feigenson, G. W. *Nat. Rev. Mol. Cell. Biol.* **2008**, *9*, 112–124.

(2) Sud, M.; Fahy, E.; Cotter, D.; Brown, A.; Dennis, E. A.; Glass, C. K.; Merrill, A. H.; Murphy, R. C.; Raetz, C. R. H.; Russell, D. W.; Subramaniam, S. Nucleic Acids Res. **2007**, *35*, D527−D532.

(3) Schiller, J.; Suss, R.; Fuchs, B.; Muller, M.; Zschornig, O.; Arnold, K. *Future Lipidol.* **2007**, *1*, 115–125.

(4) Hankin, J. A.; Barkley, R. M.; Murphy, R. C. *J. Am. Soc. Mass. Spectrom.* **2007**, *18*, 1646–1652.

(5) Petkovic, M.; Vocks, A.; Muller, M.; Schiller, J.; Arnhold, E. *Z. Naturforsch. (C)* **2005**, *60*, 143–151.

(6) Petkovic, M.; Schiller, J.; Muller, M.; Benard, S.; Reichl, S.; Arnold, K.; Arnhold, J. *Anal. Biochem.* **2001**, *289*, 202–216.

(7) Schiller, J.; Zschornig, O.; Petkovic, M.; Muller, M.; Arnhold, J.; Arnold, K. *J. Lipid Res.* **2001**, *42*, 1501–1508.

(8) Fuchs, B.; Schober, C.; Richter, G.; Suss, R.; Schiller, J. *J. Biochem. Biophys. Methods* **2007**, *70*, 689–692.

(9) Schiller, J.; Suss, R.; Arnhold, J.; Fuchs, B.; Lessig, J.; Muller, M.; Petkovic, M.; Spalteholz, H.; Zschornig, O.; Arnold, K. *Prog. Lipid Res.* **2004**, *43*, 449–488.

(10) Jones, J. J.; Borgmann, S.; Wilkins, C. L.; O'Brien, R. M. *Anal. Chem.* **2006**, *78*, 3062–3071.

(11) Caprioli, R. M.; Farmer, T. B.; Zhang, H. Y.; Stoeckli, M. *Abstr. Pap. Am. Chem. Soc.* **1997**, *214*, 113-ANYL.

(12) Caprioli, R. M.; Farmer, T. B.; Gile, J. *Anal. Chem.* **1997**, *69*, 4751–4760.

10.1021/ac801662n CCC: $40.75
Published on Web 10/30/2008

experiment, i.e., the anatomical precise localization of the biological molecules in the tissue. Such information can be crucial to specifically locate biomarkers related to pathologies like cancer or metabolic disorders. The technique also allows a direct comparison between the spectra of normal and damaged tissue, facilitating the identification of species related to the disease, and to correlate ion images with histological findings observed by light microscopy. This spatial information is especially relevant in organs such as the brain, where the cells and neuronal networks are specialized in discrete nuclei or brain areas that control or regulate the physiology of mental processes.

In an IMS experiment, a portion of tissue is placed on a matrix-assisted laser desorption/ionization (MALDI) plate and covered with a suitable matrix. The plate is introduced in the spectrometer at high vacuum and scanned, recording spectra every few micrometers. Each spectrum covers a wide region of masses, centered on the species of interest, typically 300−1800 Da in the case of lipids. Employing adequate software, it is possible to obtain density maps of the species of interest, representing the intensity of each mass channel against the coordinates at which the spectra are recorded. A huge amount of information is obtained in each experiment, as many species can be identified in each spectrum. Besides, the resulting images allow easy identification of the areas in which the relative abundance of the species of interest is located.

However, several difficulties must be overcome to successfully carry out IMS experiments. One of the most relevant issues is to obtain a uniform layer of matrix crystals on the whole surface of the tissue extract or slice. As the signal intensity strongly depends on the matrix/analyte concentration ratio, fluctuations in the deposition of the matrix result in poor reproducibility of the results from one sample to another. Several techniques have been reported to ensure a uniform matrix deposition, including the use of an inkjet printer[15] and the sublimation of the matrix under vacuum conditions.[4] Nevertheless, one of the most popular is the employment of a more or less sophisticated spray. Another and even more relevant issue is the election of the right substance as a matrix. The whole MALDI process relies on the ability of the matrix to vaporize when irradiated with the ablation laser, releasing the analytes intact into the extraction region of the spectrometer. At the same time, the fragmentation of the matrix must present the right pH: when a neutral substance is to be observed, an acid matrix must be employed so it can release H^+ during the ablation process that will attach to the analytes. The charged analytes can be accelerated by the field in the ionization region and directed toward the detector. On the other hand, if the analytes are already charged, the employment of a neutral matrix is usually better. In addition, the matrix must not be amenable to polymerization and its fragments must not overlap with the region of masses of interest.

The study and identification of lipids is a special and complicated case, due to their large variety of classes, subclasses, and molecular species (for a classification, see http://www.lipidmaps.org): generally hydrophobic in nature, but with hydrophobic and hydrophilic, charged and uncharged elements that constitute the lipid. In addition, the difference in the concentration of lipid components within a given sample is enormous. Therefore, it is not simple to find a suitable matrix for the detection of a number of them simultaneously in a given biological sample. The two most typically employed matrixes are 2,5-dihydroxyacetophenone (DHA) and 2,5-dihydroxybenzoic acid (DHB).[16] DHB is a widely used matrix for lipid analysis, although it tends to form large crystals, where the analyte is not evenly distributed, leading to poor spot-to-spot reproducibility and lowering mass resolution.[17] DHA is also well suited to the detection of lipids, but it sublimates under high-vacuum conditions, preventing detection after a short period of time.[18,19] Some studies have been published in which several substances were explored as an alternative to the matrixes traditionally employed for peptides. Among them, 4-paranitroaniline (PNA) seems to be an excellent option for detection of a wide range of lipids.[20] However, it presents the same drawback as DHA, a high vapor pressure. In this study, several substances were tested as matrixes for the detection of lipid species, mainly in the molecular weight range of phospholipids, which constitute the most abundant class of lipids in the brain and liver. Consequently, the assays were performed on rat cerebellum and on liver lipid extracts and directly on tissue cryostat sections, although for the sake of brevity, only the results obtained with the best matrix candidate found will be presented. 2-Mercaptobenzothiazole (MBT), which has already been reported to work well for the detection of large proteins,[21] allowed the detection and identification (with an accuracy of ~10 ppm) of a wide variety of lipids, in both positive and negative modes. Its low vapor pressure, due to its higher molecular weight, allows acquisition times of hours, and this makes it possible to scan tissue slices to create well-defined mass images, although at a lower accuracy than in extracts (~80 ppm), with our experimental arrangement.

EXPERIMENTAL METHODS

Animals, Tissue Sectioning, and Lipid Extraction. Animal care and research protocols were carried out according to guidelines approved by the Institution's ethical committee following Spanish legislation (RD 1201/2005) and the internationally accepted directives (86/609/EEC). All experiments were performed on adult pathogen-free Sprague−Dawley rats. Partial hepatectomy (70%) was performed on ether-anaesthetized animals as described previously,[22] and the remnant liver mass was removed 24 h later. Freshly isolated pieces of quiescent and regenerating liver were washed with cold saline and either immediately used for lipid extraction or frozen by immersion in liquid nitrogen-cooled isopentane, before storage at −80 °C. To obtain the brain tissue, after being anaesthetized with chloral hydrate (400 mg/kg, ip), the animals were decapitated and their

(13) Garrett, T. J.; Yost, R. A. *Anal. Chem.* **2006**, *78*, 2465–2469.
(14) Landgraf, R. R.; Garrett, T. J.; Calcutt, N. A.; Stacpoole, P. W.; Yost, R. A. *Anal. Chem.* **2007**, *79*, 8170–8175.
(15) Baluya, D. L.; Garrett, T. J.; Yost, R. A. *Anal. Chem.* **2007**, *79*, 6862–6867.
(16) Schiller, J.; Arnhold, J.; Benard, S.; Muller, M.; Reichl, S.; Arnold, K. *Anal. Biochem.* **1999**, *267*, 46–56.
(17) Bouschen, W.; Spengler, B. *Int. J. Mass Spectrom.* **2007**, *266*, 129–137.
(18) Wang, H. Y. J.; Jackson, S. N.; Woods, A. S. *J. Am. Soc. Mass Spectrom.* **2007**, *18*, 567–577.
(19) Jackson, S. N.; Ugarov, M.; Egan, T.; Post, J. D.; Langlais, D.; Schultz, J. A.; Woods, A. S. *J. Mass Spectrom.* **2007**, *42*, 1093–1098.
(20) Estrada, R.; Yappert, M. C. *J. Mass Spectrom.* **2004**, *39*, 412–422.
(21) Xu, N. X.; Huang, Z. H.; Watson, J. T.; Gage, D. A. *J. Am. Soc. Mass Spectrom.* **1997**, *8*, 116–124.
(22) Waynforth H. B., Flecknell P. A. *Experimental and surgical technique in the rat*; Academic Press: New York, 1992.

brains were rapidly removed, dissected at 4 °C, and kept at −80 °C until used. Frozen brains and livers were sectioned (12-μm thickness) at −25 °C in a cryostat (Microm, HM550). Serial sagittal sections were obtained from the cerebellum. The orientation of the liver was arbitrary. Tissue sections were mounted on microscope cover slides (24 × 40 mm, Menzel-Glaser) and kept at −25 °C until they were fixed onto a MALDI metal holder (Bruker Daltonics) modified to hold the cover slide. Sections consecutive to those on the slides were stained with cresyl violet, and a rat brain atlas was used for the assignment of the brain region analyzed by MS.

Pieces of liver and cerebellum were homogenized at 4 °C in 5 volumes of ice-cold phosphate buffer solution pH 7.4 using a Polytron (Kinematica) homogenizer,[23] and protein concentration in homogenates was determined using Pierce reagent. Lipids were exhaustively extracted from homogenates by a modified Bligh and Dyer[24] procedure described earlier;[25] the solvent was removed in a Savant SpeedVac concentrator−evaporator, the lipids were dissolved in toluene, and the extracts were stored under N_2 atmosphere at −80 °C until analyzed.

Sample Preparation for MALDI-TOF. The following matrixes (MALDI quality from Sigma-Aldrich, St. Louis, MO) were employed: 0.5 M DHB + 0.1% trifluoroacetic acid; 1-isoquinolinol (sat); 1,8,9-anthracenetriol (sat); DHA (sat); PNA (sat); and MBT (sat). Matrixes were dissolved in methanol. Saturated solutions of MBT, DHB, PNA, and DHA were prepared to visualize crystallization differences, using the same procedure described in Sample Preparation for IMS.

The following lipid standards were used as commercial samples to assess the performance of the matrixes and for identification: bovine liver glycerophosphocholines (GPCho), glycerophosphoethanolamines (GPEtn), and glycerophosphoinositols (GPIns); porcine brain sphingomyelins (SPM) and glycerophosphoserines (GPSer); bovine heart cardiolipin; synthetic lysoglycerophosphocholines; and egg diolein (diacylglycerol, DAG) and L-glycerophosphoglycerols (GPGro) were obtained from Avanti Polar Lipids (Alabaster, AL). Cholesterol, triolein (triacylglycerol, TAG), and cholesteryl oleate were from Sigma-Aldrich.

Lipid standards were diluted in chloroform at 1 mg/mL concentration and mixed in a 1:1 (v/v) ratio with matrix solution. One microliter of the resulting solution was spotted in every target well. Tissue lipid extracts with a total lipid concentration of ∼10 mg/mL were mixed with the matrix solution in a 1:10 (v/v) ratio in order to adjust total lipid concentration to ∼1 mg/mL. One microliter of the mixture was spotted in each well of the stainless steel target plate and cocrystallized by evaporation.

Spectra were acquired in either positive or negative linear and reflectron modes with the aid of a Bruker (Bremen, Germany) Reflex IV time-of-flight mass spectrometer, employing different sets of voltages for the ion source in order to focus the adequate mass range. 300 shots were accumulated for each spectrum of extracts, and at least 10 replicates of each extract were analyzed to assess reproducibility of the spectra.

Accurate Mass Determination. The use of delayed extraction in MALDI-TOFMS distorts the relationship between linear m/z and squared time-of-flight (t^2). In addition, there is a relative error associated with the position of the sample in the plate, which is directly proportional to m/z. To minimize such errors, a two-step recalibration procedure similar to the one developed by Gobom and co-workers[26] was applied to the low-mass range of the spectra as follows. The first step involves the use of a high-order polynomial to externally calibrate the masses. To get the constants of the external calibration polynomial, 36 peaks of the poly(ethylene glycol)-sodium adduct $[PEG\text{-}Na]^+$ spectrum in the range 400−2000 Da, obtained in various positions of the target plate surrounding the sample, were used and fitted to 15−25 degree polynomials, with the 19-degree polynomial providing the best fit. The second step consists of internally correct the remaining relative error by means of a linear regression using well-known masses in the spectrum of interest. In this way, an ∼10 ppm accuracy in mass determination is achieved.

Peak Assignment. The samples analyzed in this paper are quite complex, due to the large number of lipids that share similar masses. Without the employment of MS/MS, it is not possible to discriminate chemical variants of lipids with identical numbers of acylic carbons and double bonds, that is, with identical masses. Therefore, the identity of the alkyl chains and the position of their double bonds cannot be specified in this study. The assignment of lipid species was facilitated by the employment of a database created using tissue-dependent lipid composition and the alkyl composition of standards offered by the suppliers. The experimental values of the peaks' positions were compared with this database and with the data in Lipid MAPS (http://www.lipidmaps.org/)[2] and Madison Metabolomics Consortium (http:mmcd.nmrfam.wisc.edu/)[27] databases, using the mass accuracy as a tolerance window. In this way, a single candidate for each peak in the spectrum was obtained in most cases. The glycerolipid species numbers (*x*:*y*) denote the total length and number of double bonds of acyl chains, while the sphingolipid and sulfatide species numbers correspond to the length and number of double bonds of the acyl chain added to those of the attached sphing-4-enine (d18:1) or sphinganine (d18:0) base.

Sample Preparation for IMS. The tissue was placed over a glass cover slide, which was attached to the target with sticky tape. A tracing paper was placed under the sample to position it in the scanning area. The most delicate part of the sample preparation is the matrix deposition. A uniform coat of matrix was applied using a sprayer (DESAGA, model SG1B), loaded with an MBT/methanol saturated solution. The matrix was sprayed from a 50-cm distance, exposing the sample only when the sprayer was in stationary regimen. Up to 20 spraying/dying cycles were employed in order to obtain a uniform layer. The same spraying procedure was employed to obtain micrographies of the crystallized matrixes with an Axioscop Zeiss microscope using bright-field diffraction by phase contrast.

(23) Palacios, L.; Ochoa, B.; Gomez-Lechón, M. J.; Castell, J. V.; Fresnedo, O. *Biochim. Biophys. Acta Mol. Cell Biol. Lipids* **2006**, *1761*, 698–708.
(24) Bligh, E. G.; Dyer, W. J. *Can. J. Biochem. Physiol.* **1959**, *37*, 911–917.
(25) Ruiz, J. I.; Ochoa, B. *J. Lipid Res.* **1997**, *38*, 1482–1489.
(26) Gobom, J.; Mueller, M.; Egelhofer, V.; Theiss, D.; Lehrach, H.; Nordhoff, E. *Anal. Chem.* **2002**, *74*, 3915–3923.
(27) Cui, Q.; Lewis, I. A.; Hegeman, A. D.; Anderson, M. E.; Li, J.; Schulte, C. F.; Westler, W. M.; Eghbalnia, H. R.; Sussman, M. R.; Markley, J. L. *Nat. Biotechnol.* **2008**, *26*, 162–164.

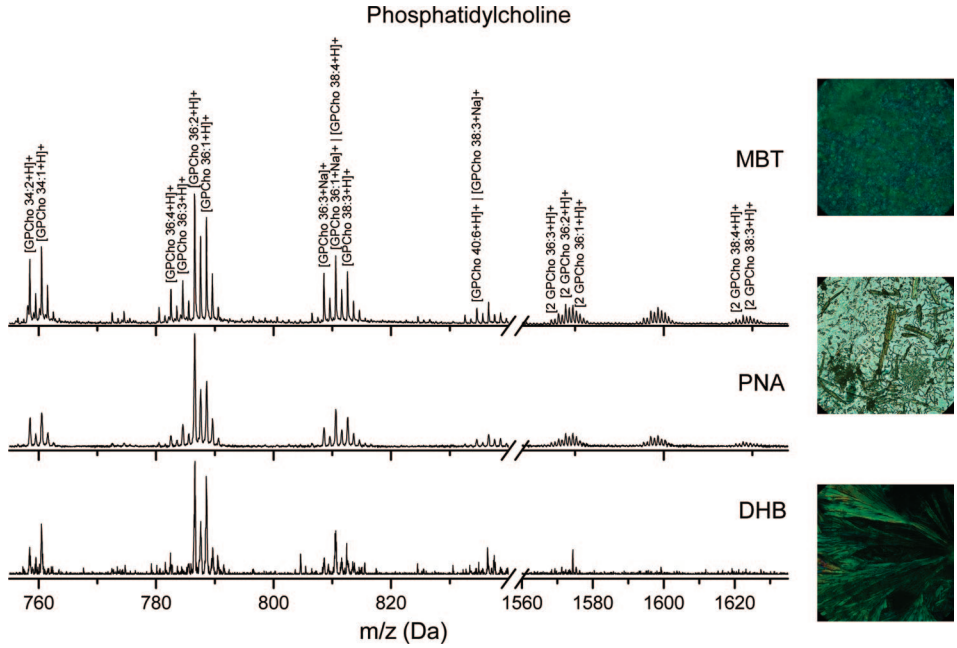

Figure 1. MALDI-TOF mass spectra of a glycerophosphocholine standard taken with DHB, PNA, and MBT matrixes in positive ion reflectron mode. Each spectrum is the average of 300 shots in random locations along the sample. The absolute intensity of the highest peak on the spectra (GPCho 36:2) is 180, 2880, and 7393 for DHB, PNA, and MBT, respectively. The assignment of the most relevant peaks in the spectrum is indicated. On the right of each spectrum it is shown a microscope image (original magnification 400×) of the corresponding matrix crystals of an IMS sample preparation.

The definition of the acquisition area was performed with CreateTarget,[28] generating files in a format compatible with the Bruker Reflex IV spectrometer. Thirty shots on a single location are accumulated to construct every spectrum, with a total acquisition time of 2−9 h, depending on the size of the scanned area. The spatial resolution of all the mass images shown in this work was 100 μm. As there is a shift in the masses across the tissue, acquired spectra were aligned maximizing correlation with the overall averaged spectrum, normalized by using the total ion current and exported to a Histomass compatible format using a script written in Mathematica 6.0. This processing step takes no longer than 20 min. The data analysis and visualization was carried out with Histomass, a powerful computer program created specifically for the graphical evaluation of data from IMS experiments (http://www.noraybio.com/en/histomass.asp).

RESULTS AND DISCUSSION

Figure 1 shows the mass spectrum of a GPCho standard taken in reflectron mode, using three different matrixes, DHB (lower), PNA (middle), and MBT (upper trace), together with their corresponding microscopic crystallization (original magnification 400×). The same spectra were recorded with the other matrixes listed in Experimental Methods, obtaining a less favorable S/N ratio. As already stated in the introduction, DHB is considered as the standard matrix for lipid studies. However, the spectra obtained with PNA offer a better S/N ratio, especially for GPCho dimers. The upper trace shows the spectrum obtained using MBT. As can be seen, MBT yields high-quality results, with narrower peaks. The better S/N ratio obtained with this matrix allows the identification of even low-abundance species such as, for example, those around 800 Da, which are undistinguishable with the other two matrixes. This is a very important issue in, for example, studies aimed at finding disease markers, where it is desirable to follow the behavior of the maximum number of lipid species. The major drawback of this matrix is a large fragmentation pattern that precludes the detection of species with molecular masses below ∼500 Da, although this can be partly overcome by the formation of ^{132}Cs adducts. In this way, lipids in the ∼300−500 Da mass range are shifted toward the more convenient 500−700 Da window, where they are easily detected. Therefore, the detection of DAG, lysoderivatives, and cholesterol and related lipids needs the generation of ^{132}Cs adducts or the employment of another matrix. The microscopic images in Figure 1 show that MBT forms small, uniform crystals when compared with PNA and DHB, in an IMS sample preparation. This is another important advantage for the recording of IMS data, where the size of the matrix crystals is one of the determinant parameters to achieve a good spatial resolution and uniform spectra all over the tissue slice.

The species on the spectra of Figure 1 were identified based on their mass, which was determined with an accuracy of ∼10 ppm (standard deviation) using the procedure described above for calibration, and by comparison with the alkylic composition offered by the supplier.

In addition to a better S/N ratio, MBT offers longer acquisition times than PNA, as seen in Figure 2, where spectra of rat cerebellum lipid extracts acquired with PNA (Figure 2A) or MBT (Figure 2B) matrixes at different times after introducing the sample in the spectrometer are shown. Due to the high vapor pressure of PNA, the signal intensity of the spectra in Figure 2A remains constant for less than 45 min. At that acquisition time, the change in the relative intensity of some of the species is

(28) Clerens, S.; Ceuppens, R.; Arckens, L. *Rapid Commun. Mass Spectrom.* **2006**, *20*, 3061–3066.

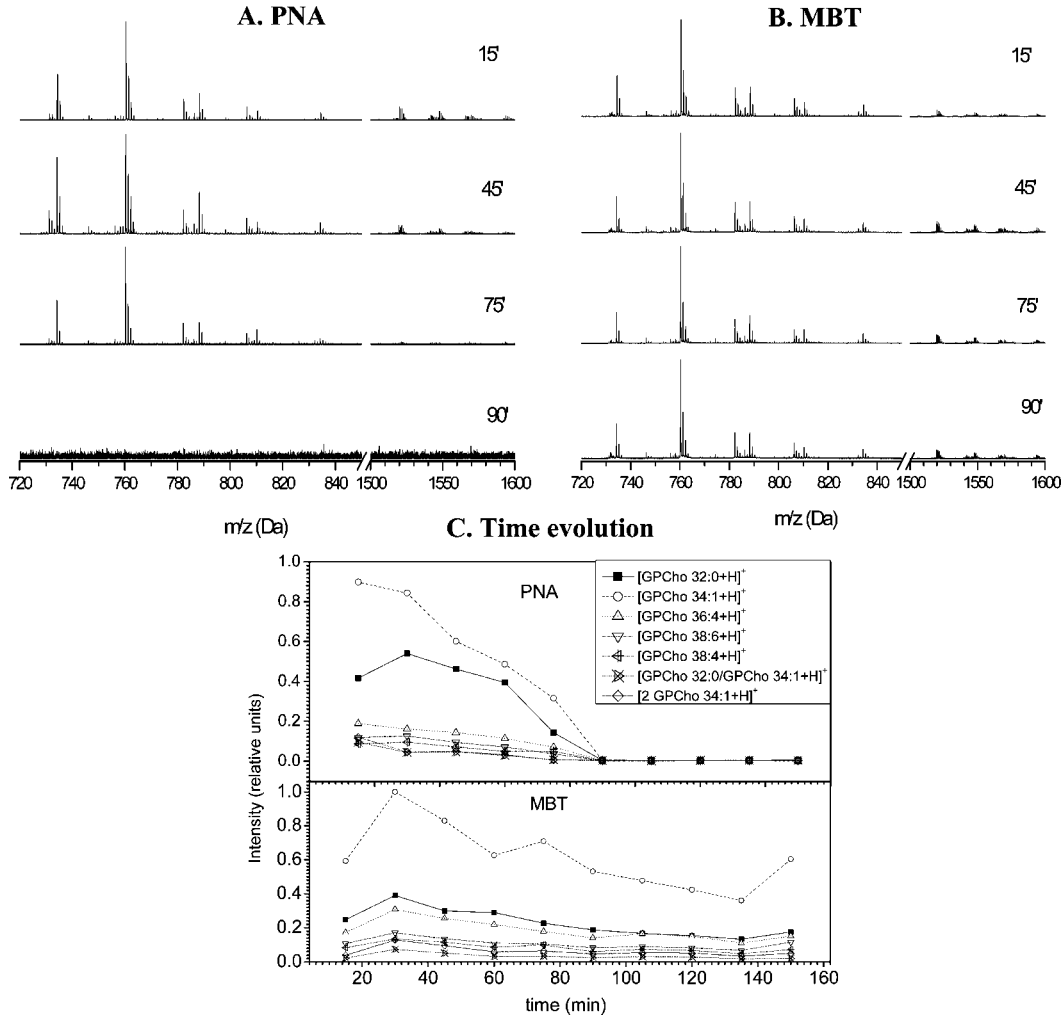

Figure 2. MALDI-TOF mass spectra of rat cerebellum lipid extracts recorded over 90 min with PNA (A) and MBT (B) matrixes in positive ion reflectron mode. In (C), intensity evolution of the main peaks on the spectra of the upper panels.

already evident. Such behavior is due to a variation of the analyte/matrix relative concentration and is a very undesirable effect, especially in studies aimed at the relative quantification of the species in the sample. At 60 min after the introduction of the sample (Figure 2C), the signal of some of the species had dropped ~50%, due to the evaporation of the matrix. At 90 min, no signal at all was detected (not even from the matrix alone) due to its complete sublimation. Even less favorable results were obtained with DHA and DHB, but those results are not shown here for the sake of brevity. On the other hand, the spectra taken with MBT (Figure 2B) show no variation with time up to 150 min. During that time, the relative intensity of the peaks remains constant within the experimental error, and no variation in the S/N ratio is appreciated, in contrast to that observed with PNA (Figure 2C). This key feature enables analysis of a larger number of samples in a single experiment, without reloading the target in the spectrometer, and allows the recording of spectra of lipids directly from tissue slices, as is shown below.

MBT also offers a high reproducibility from sample to sample, due in part, to its crystallization in very small and homogeneous crystals (see insets in Figure 1). The influence of the crystal size in the intensity of the spectra is well-known; some matrixes form large crystals that lead to a very heterogeneous distribution of the sample in the well and, therefore,

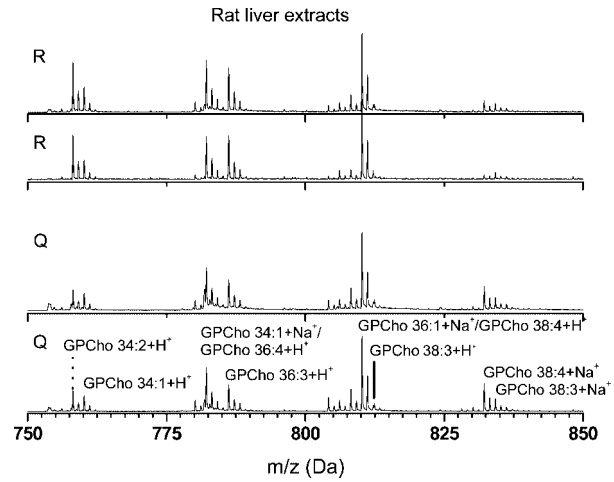

Figure 3. MALDI-TOF mass spectra of (Q) quiescent and (R) regenerating liver lipid extracts with MBT matrix in positive ion reflectron mode. Samples correspond to two different animals. For a complete list of identified species see Table 1.

make it necessary to scan the whole sample to obtain an average spectrum, making them useless for mass imaging purposes. Figure 3 shows the 750−850 Da range of four spectra of rat liver lipid extracts obtained with MBT. The two lower

traces correspond to two different samples of lipid extracts from quiescent rat liver (Q), while the two upper traces correspond to two different samples of regenerating liver (R), which exemplifies both hepatic steatosis and normal hepatocyte cell proliferation. As can be seen from the R/R and Q/Q comparisons, there is a high reproducibility of the spectra. The relative intensity and overall aspect of the R/R and Q/Q spectra is preserved from one sample to another. Such a high reproducibility and the excellent quality of the spectra allow the identification of variations between regenerating and quiescent samples, even without the introduction of an internal standard. For example, the GPCho 38:4 and 38:3 species have a higher relative abundance in sample Q, while the GPCho 34:2 and GPCho 34:1 relative abundance is higher in sample R. Also, the intensity of the peak at m/z 804.567 (GPCho 36:4) greatly decreases from the quiescent to the regenerating samples' spectra. These changes, which are in close agreement with the decreased levels of long-chain polyunsaturated fatty acids that were observed in liver regeneration and hepatocarcinogenesis,[29] suggest that liver regeneration is associated with marked changes in the fatty acyl molecular species that are incorporated into defined glycerophospholipids.

Table 1 collects all the species identified in liver extracts in positive mode (for the species identified in negative mode, see Supporting Information (SI) Table S-1). The assignment was performed following the procedure in the Experimental Section. For the sake of brevity, the spectra in negative mode are not shown but a large number of species were identified due to an excellent S/N ratio obtained with MBT (see SI Table S-1). More than half of the lipids detected in positive mode correspond to GPCho, which produces strong signals due to its permanent positive charge. Thus, 20 different species of GPCho, 4 species of lysoGPCho, 6 species of GPEtn, 2 SPM, and 5 GPIns were detected in positive mode, forming different adducts with H^+, Na^+, and Cs^+. The species detected and identified in the dimers region are also collected in Table 1, although they do not lead to the identification of new monomers. The addition of CsCl to the sample to form Cs adducts shifts the peaks 132 Da to higher masses, which is very useful to detect species with masses below ~500 Da. Moreover, the GPEtn species were only detected after the addition of CsCl.

The low acidity of the matrix employed also allows the application of negative mode detection, which results in the identification of several additional species, although the total number is smaller than for positive detection. Fifteen GPCho, 10 GPIns, 4 GPEtn, and 3 GPSer are detected in negative mode. GPCho species are only detected after capture of an OH group, otherwise, the natural charge of those phospholipids precludes their detection. The number of GPIns species detected in negative mode is considerably larger than in positive mode, in agreement with previous findings (see Table S-1, SI).[9]

Figure 4 shows the 720−850//1500−1600 Da mass ranges of a rat cerebellum extract spectrum, taken in positive ion reflectron mode (upper panel), and a spectrum of the same sample, taken in negative mode, both using MBT matrix. Some of the major mass peaks in both spectra are labeled, demonstrating that a large number of species is detected in both positive and negative modes. It is well-known that the employment of different matrixes leads to the identification of different classes of lipids. As an example, a matrix formed by gold

Table 1. Lipid Species Identified in Liver Extracts from Mass Spectra Recorded in Positive Mode Using MBT as a Matrix[a]

experimental mass	theoretical mass	assignment		
520.329	520.340	LysoGPCho	{18:2}	$[M+H]^+$
524.382	524.372	LysoGPCho	{18:0}*	$[M+H]^+$
544.328	544.338	LysoGPCho	{18:1}	$[M+Na]^+$
	544.340	LysoGPCho	{20:4}	$[M+H]^+$
732.548	732.554	GPCho	{32:1}*	$[M+H]^+$
754.535	754.536	GPCho	{32:1}	$[M+Na]^+$
	754.540	GPCho	{34:4}	$[M+H]^+$
756.552	756.554	GPCho	{34:3}*	$[M+H]^+$
758.568	758.570	GPCho	{34:2}*	$[M+H]^+$
760.579	760.586	GPCho	{34:1}*	$[M+H]^+$
772.583	772.586	GPEtn	{38:2}	$[M+H]^+$
780.561	780.552	GPCho	{34:2}	$[M+Na]^+$
	780.550	GPCho	{36:5}*	$[M+H]^+$
782.574	782.568	GPCho	{34:1}	$[M+Na]^+$
	782.570	GPCho	{36:4}*	$[M+H]^+$
784.585	784.586	GPCho	{36:3}	$[M+H]^+$
786.606	786.601	GPCho	{36:2}*	$[M+H]^+$
788.619	788.617	GPCho	{36:1}*	$[M+H]^+$
796.565	796.526	GPCho	{34:2}	$[M+K]^+$
	796.590	GPEtn	{40:4}	$[M+H]^+$
797.575	797.557	SPM	{40:7}	$[M+Na]^+$
798.566	798.542	GPCho	{34:1}	$[M+K]^+$
804.567	804.552	GPCho	{36:4}	$[M+Na]^+$
806.573	806.568	GPCho	{36:3}*	$[M+Na]^+$
	806.570	GPCho	{38:6}*	$[M+H]^+$
808.603	808.583	GPCho	{36:2}	$[M+Na]^+$
	808.590	GPCho	{38:5}*	$[M+H]^+$
810.614	810.599	GPCho	{36:1}	$[M+Na]^+$
	810.600	GPCho	{38:4}*	$[M+H]^+$
812.618	812.617	GPCho	{38:3}*	$[M+H]^+$
814.589	814.560	GPSer	{38:3}	$[M+H]^+$
822.569	822.542	GPCho	{36:3}	$[M+K]^+$
824.587	824.557	GPCho	{36:2}	$[M+K]^+$
830.579	830.568	GPCho	{38:5}	$[M+Na]^+$
832.605	832.583	GPCho	{38:4}	$[M+Na]^+$
834.615	834.599	GPCho	{38:3}	$[M+Na]^+$
	834.600	GPCho	{40:6}*	$[M+H]^+$
835.476	835.473	SPM	{34:1}	$[M+Cs]^+$
836.622	836.615	GPCho	{38:2}*	$[M+Na]^+$
	836.620	GPCho	{40:5}*	$[M+H]^+$
848.575	848.557	GPCho	{38:4}	$[M+K]^+$
862.438	862.436	GPCho	{32:2}	$[M+Cs]^+$
876.449	876.452	GPEtn	{36:2}	$[M+Cs]^+$
899.521	899.505	GPIns	{36:3}	$[M+K]^+$
900.425	900.452	GPEtn	{38:4}	$[M+Cs]^+$
904.462	904.483	GPEtn	{38:2}	$[M+Cs]^+$
915.808	915.838	TAG	{56:2}	$[M+H]^+$
916.477	916.483	GPCho	{36:3}	$[M+Cs]^+$
921.514	921.490	GPIns	{38:6}	$[M+K]^+$
925.499	925.521	GPIns	{38:4}	$[M+K]^+$
926.488	926.468	GPEtn	{40:5}	$[M+Cs]^+$
928.517	928.483	GPEtn	{40:4}	$[M+Cs]^+$
929.757	929.757	TAG	{56:6}	$[M+Na]^+$
949.511	949.521	GPIns	{40:6}	$[M+K]^+$
951.552	951.536	GPIns	{40:5}	$[M+K]^+$
1516.11	1516.13	GPCho	{34:2}	$[2M+H]^+$
1540.12	1540.13	GPEtn	{38:3}	$[2M+H]^+$
1544.15	1544.16	GPEtn	{38:2}	$[2M+H]^+$
1564.13	1564.13	GPCho	{36:4}	$[2M+H]^+$
1568.16	1568.16	GPCho	{36:3}	$[2M+H]^+$
1572.19	1572.19	GPCho	{36:2}	$[2M+H]^+$
1592.17	1592.16	GPEtn	{40:4}	$[2M+H]^+$
1616.18	1616.16	GPCho	{38:5}	$[2M+H]^+$
1620.21	1620.19	GPCho	{38:4}	$[2M+H]^+$

[a] The species with an asterisk appear also with Cs, but their Cs adducts are omitted for brevity.

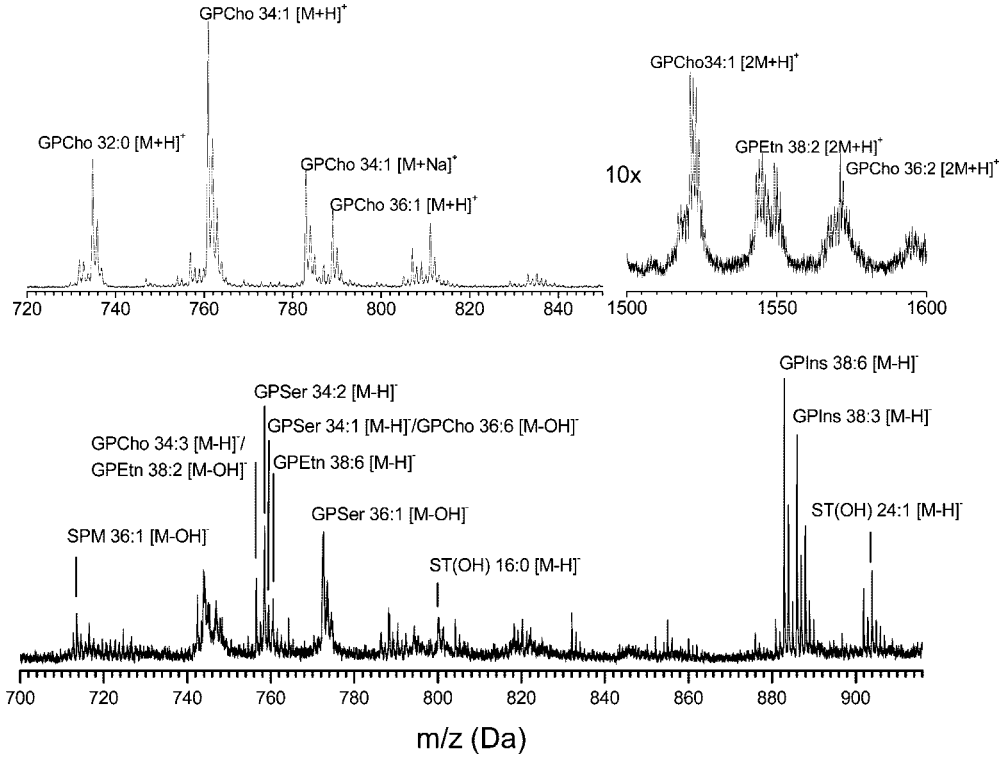

Figure 4. MALDI-TOF mass spectra of cerebellum lipid extracts with MBT matrix in positive (upper panels) and negative (lower panel) ion reflectron modes. For a complete list of identified species see Table 2 (and Table S-2, SI).

nanoparticles enables detection and imaging of cerebrosides in rat brain tissue,[30] which are not seen when using an organic matrix such as DHB or MBT. Table 2 collects the species identified in cerebellum extracts in positive mode together with the references to those lipid species reported in previous studies (see Table S-2 (SI) for the species identified in negative mode).[31−35] Altogether, 43 species are detected in positive mode, while 16 different species are detected in negative mode. Therefore, with the employment of MBT as a matrix, a larger number of species is detected than with DHA, DHB, or even PNA. In addition to the detection of the most abundant GPCho, GPEtn, GPSer, and GPIns species in the brain, it is noteworthy that several lysoGPCho and TAG, and even several DAG and sulfatides (ST) species were detected without the application of any previous separation procedure.

The employment of a long acquisition time matrix as MBT extends the field of IMS to lipids (Figure 5, for rat cerebellum; Figure S-1, SI, for rat liver). Using the IMS analysis in rat liver sections (~8 × 5 mm and 12 μm thickness) we identified different lipid species; i.e., representing the intensity of GPCho 36:1+Na^+ mass channel for each spectrum against the coordinates at which they were recorded in positive mode, we obtained the color-coded image shown in Figure S-1 (SI). A representative spectrum of those employed to compose the image, with the mass channel represented in the mass image highlighted in red is also presented. The mass range recorded in liver sections was m/z 0−1800, but no ions with significant abundance appeared above m/z 900. The spectra were taken with 100-μm spacing, resulting in 4000 spectra and a ~4-h acquisition time.

The obtained images reveal a rather non-prevalent distribution of the ion at m/z 810.6 Da within the tissue, as expected from a normal lobule of the liver parenchyma where discrete histological areas cannot be appreciated at such resolution (Figure S-1, SI). The uniform intensity distribution is a further proof of the temporal signal stability achieved with MBT. The most relevant lipid species identified in liver extracts are present in tissue slices, but in addition, other lipid species and a diversity of metabolites with masses within the recorded range may also be present, making the peak assignment more difficult. The comparison with the spectra in Figure 3 supports the direct identification of several GPCho species, like GPCho 34:2, 34:1+Na^+, and 36:1+Na^+//38:4+H^+, but the spectra obtained from the slices show additional peaks, some of them of high intensity, like the ion at m/z 860.66 ± 0.05 Da, whose molecular weight is consistent with GPCho 40:4+Na^+.

It is important to note that the mass accuracy of the spectra recorded in situ from the tissue is somewhat lower than those recorded from extracts, being ~80 ppm. Two causes may likely account for such a loss of accuracy. One, the lipids are desorbed from a 12-μm-thick tissue section, which moreover may present some kind of roughness, so that the lipids at different depths in

(29) Abel, S.; Smuts, C. M.; de Villiers, C.; Gelderblom, W. C. A. *Carcinogenesis* **2001**, *22*, 795–804.
(30) Trim, P. J.; Atkinson, S. J.; Princivalle, A. P.; Marshall, P. S.; West, A.; Clench, M. R. *Rapid Commun. Mass Spectrom.* **2008**, *22*, 1503–1509.
(31) Ma, X.; Liu, G.; Wang, S.; Chen, Z.; Lai, M.; Liu, Z.; Yang, J. *J. Chromatogr., B* **2007**, *859*, 170–177.
(32) Jackson, S. N.; Wang, H. Y. J.; Woods, A. S. *J. Am. Soc. Mass Spectrom.* **2005**, *16*, 133–138.
(33) Jackson, S. N.; Wang, H. Y. J.; Woods, A. S. *J. Am. Soc. Mass Spectrom.* **2005**, *16*, 2052–2056.
(34) Jackson, S. N.; Wang, H. Y. J.; Woods, A. S. *J. Am. Soc. Mass Spectrom.* **2007**, *18*, 17–26.
(35) Jackson, S. N.; Wang, H. Y. J.; Woods, A. S. *Anal. Chem.* **2005**, *77*, 4523–4527.

Table 2. Lipid Species Identified in Cerebellum Extracts from Mass Spectra Recorded in Positive Mode Using MBT as a Matrix[a]

other works reference → species	experimental mass	theoretical mass	assignment		
	518.327	518.322	LysoGPCho	{16:0}	$[M+Na]^+$
	522.352	522.356	LysoGPCho	{18:1}	$[M+H]^+$
	524.387	524.372	LysoGPCho	{18:0}	$[M+H]^+$
	628.236	628.238	LysoGPCho	{16:0}	$[M+Cs]^+$
	652.529	652.543	DAG	{40:6}	$[M+H\text{-}OH]^+$
		652.545	DAG	{42:8}	$[M\text{-}NaOH]^+$
	718.544	718.539	GPEtn	{34:1}	$[M+H]^+$
	730.629	732.666	TAG	{46:4}	$[M\text{-}NaOH]^+$
refs 31−33, 35	731.595	731.607	SPM	{36:1}	$[M+H]^+$
	732.556	732.554	GPCho	{32:1}	$[M+H]^+$
	732.650	732.460	TAG	{46:3}	$[M\text{-}NaOH]^+$
refs 31−33, 35, GPCho 32:0+H^+	734.533	734.570	GPCho	{32:0}	$[M+H]^+$
	737.519	737.512	DAG	{44:11}	$[M+Na]^+$
	744.565	744.554	GPEtn	{36:2}*	$[M+H]^+$
ref 35	746.592	746.570	GPEtn	{36:1}*	$[M+H]^+$
ref 31	753.593	753.589	SPM	{36:1}*	$[M+Na]^+$
		753.591	SPM	{38:4}	$[M+H]^+$
refs 31, 33, 35 GPCho 32:0+Na^+	756.555	756.554	GPCho	{34:3}	$[M+H]^+$
	758.556	758.570	GPCho	{34:2}	$[M+H]^+$
refs 32, 33, 35	760.586	760.586	GPCho	{34:1}*	$[M+H]^+$
ref 32 GPCho 34:0+H^+		762.6			
	767.564	767.547	SPM	{36:2}	$[M+K]^+$
ref 32 GPEtn 38:4+H^+		768.6			
refs 31−33, 35, SPM 36:0+K^+		769.6			
refs 31, 33, 35 GPCho 32:0+K^+		772.6			
	775.596	775.573	SPM	{38:4}	$[M+Na]^+$
		775.575	SPM	{40:7}	$[M+H]^+$
ref 31	782.582	782.568	GPCho	{34:1}	$[M+Na]^+$
		782.570	GPCho	{36:4}	$[M+H]^+$
	784.596	784.586	GPCho	{36:3}	$[M+H]^+$
	786.602	786.601	GPCho	{36:2}	$[M+H]^+$
refs 31−33, 35	788.623	788.617	GPCho	{36:1}*	$[M+H]^+$
ref 32 GPEtn 40:6+H^+		792.6			
refs 31, 33, 35	798.561	798.542	GPCho	{34:1}	$[M+K]^+$
	804.572	804.552	GPCho	{36:4}*	$[M+Na]^+$
	806.578	806.568	GPCho	{36:3}*	$[M+Na]^+$
refs 31, 35		806.570	GPCho	{38:6}*	$[M+H]^+$
	808.581	808.583	GPCho	{36:2}*	$[M+Na]^+$
		808.586	GPCho	{38:5}*	$[M+H]^+$
	810.614	810.599	GPCho	{36:1}*	$[M+Na]^+$
refs 31, 35		810.601	GPCho	{38:4}*	$[M+H]^+$
	812.626	812.617	GPCho	{38:3}*	$[M+H]^+$
	814.618	814.633	GPCho	{38:2}*	$[M+H]^+$
ref 32 SPM 42:0+H^+		815.7			
ref 31 GPCho 39:6+H^+		820.6			
refs 31, 35, GPCho 36:1+K^+		826.6			
	832.602	832.583	GPCho	{38:4}	$[M+Na]^+$
	834.618	834.599	GPCho	{38:3}	$[M+Na]^+$
refs 31, 32, 35		834.601	GPCho	{40:6}	$[M+H]^+$
	836.639	836.615	GPCho	{38:2}	$[M+Na]^+$
		836.617	GPCho	{40:5}*	$[M+H]^+$
	852.458	852.477	GPSer	{38:6}	$[M\text{-}H+2Na]^+$
	860.523	860.539	GPSer	{38:2}	$[M\text{-}H+2Na]^+$
	861.483	861.489	SPM	{36:2}	$[M+Cs]^+$
	881.509	881.516	GPIns	{36:4}	$[M+Na]^+$
	901.573	901.532	TAG	{46:5}	$[M+Cs]^+$
	905.580	905.564	TAG	{46:3}	$[M+Cs]^+$
	905.740	905.757	TAG	{54:4}	$[M+Na]^+$
	907.524	907.531	GPIns	{38:5}	$[M+Na]^+$
	921.510	921.490	GPIns	{38:6}	$[M+K]^+$
	922.834	922.838	TAG	{60:6}	$[M\text{-}NaOH]^+$
	924.475	924.452	GPEtn	{40:6}	$[M+Cs]^+$
	926.475	926.468	GPEtn	{40:5}	$[M+Cs]^+$
	953.549	953.552	GPIns	{40:4}	$[M+K]^+$
	993.475	993.447	GPIns	{36:3}	$[M+Cs]^+$
ref 31, 2 GPCho 32:0+H^+		1468.2			
	1492.158	1492.13	GPEtn	{36:1}	$[2M+H]^+$
ref 31 GPCho 32:0+GPCho 34:1+H^+		1494.2			
ref 31	1520.160	1520.16	GPCho	{34:1}	$[2M+H]^+$
ref 31, 32 GPCho 34:1+Na^+		1542.2			
	1544.160	1544.16	GPEtn	{38:2}*	$[2M+H]^+$
ref 31 GPCho 34:1+GPCho 38:6+H^+		1566.2			
	1568.160	1568.16	GPCho	{36:3}	$[2M+H]^+$
	1572.170	1572.19	GPCho	{36:2}	$[2M+H]^+$

[a] The species with an asterisk also appear with Cs, but their Cs adducts are omitted for brevity. Comparison with the assignments in previous works using MALDI-TOF mass spectrometry is also offered. DHB was used as a matrix in refs 30 and 35, DHA in refs 32−35. In ref 32, 6-aza-2-thiotimine, α-cyano-4-hydroxycinnamic acid, and sinapinic acid are also employed.

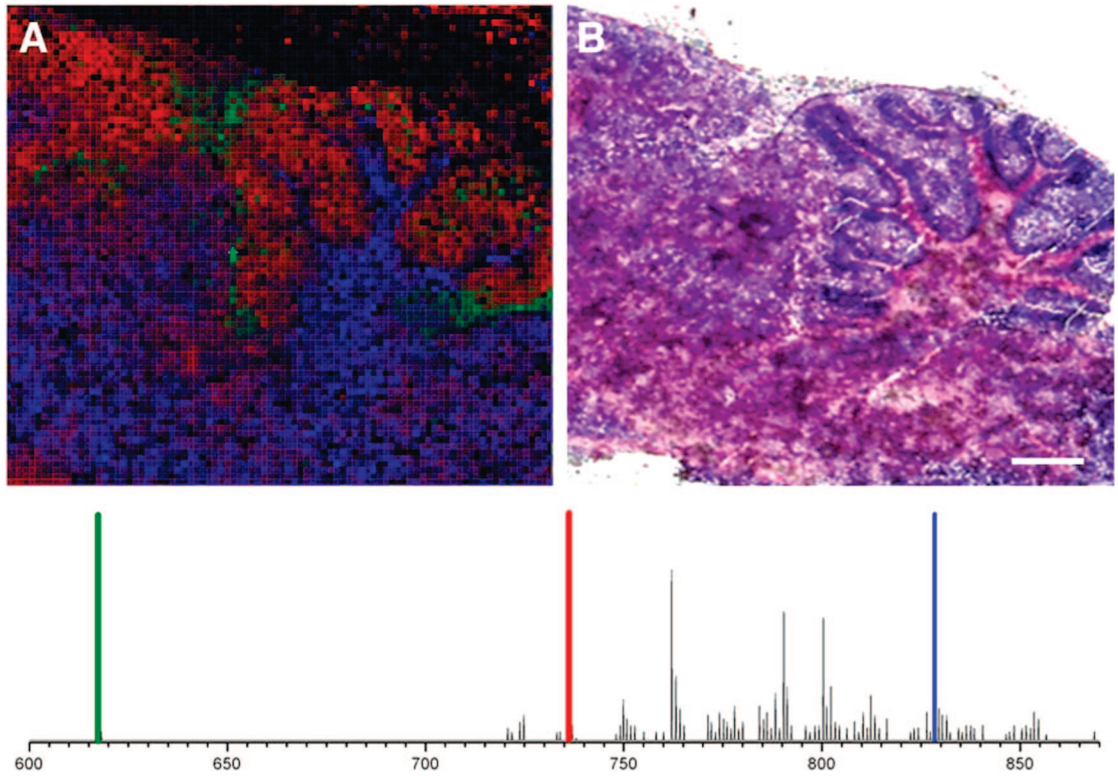

Figure 5. IMS obtained with MBT matrix and reflectron detection from a sagittal section of rat brain tissue (A), together with the Nissl-stained image for comparison and anatomical recognition (B). The sagittal section was 10 × 9 mm and the spectra were recorded with 100-μm spacing, resulting in 9000 spectra. A representative 1D mass spectrum is also shown, with the peaks employed to compose the image highlighted, using the same color code as in the image. Scale bar, 1 mm.

the tissue reach the detector at slightly different times; and two, the microenvironment from which the lipids are desorbed can be different from one part of the tissue to another, also resulting in slight changes in the time-of-flight.

Mass spectrometric images of rat brain appear with high definition and delineate fine anatomical structures. Figure 5 shows the mass image obtained with the Histomass program from a sagittal brain section at the cerebellum level (A), and the Nissl counterstaining of the same section after the MBT matrix application (B), as well as a representative mass spectrum with the peaks employed for constructing the image highlighted: GPCho 36:1+K^+ (blue squares), GPCho 32:0+H^+ (red squares) and the ion observed at m/z 615.7 Da (green squares). The sagittal section is 10 × 9 mm and the image is recorded with 100-μm spacing between spectra resulting in 9000 spectra and a ~8-h acquisition time. The spectrogram shows the typical tree shape of the rat cerebellum at its hemibrain medial part. At this resolution, it is possible to appreciate in different blue color saturations the relative abundance of GPCho 36:1 in white matter-rich areas (brain stem, cerebellar peduncles, and white matter tracts corresponding to pink staining in Figure 5B), in agreement with previous findings,[30] whereas GPCho 32:0 (red) is clearly more abundant in gray matter as can be appreciated in both the cerebral and cerebellar cortex (external part, violet staining in Figure 5B). Finally, the ependymal cells that cover the brain, including the ventricles with the choroid plexus, possess a specific molecule detected at m/z 615.7 (green). The assignment of this peak is not simple, taking into account the 80 ppm accuracy in this IMS experiments. Although exhaustive searching in databases shows several candidates for this mass, physiological reasoning narrows the possibilities to two types of compounds: a porphyrin and DAG 36:5+H^+. Ependymal cells constitute the blood−cerebrospinal fluid barrier. The possibility exists that they are enriched in specific lipid species, but the high vascularization of this area, together with the fact that this molecule is not detected in lipid extracts, support the identification of this ion as an heme derivative, such as the heme-(Fe^{3+}) previously found in brain homogenates.[10]

The differences between the spectra in the areas identified in Figure 5 can be viewed in more detail when the mass spectra of random spots inside the mentioned areas are analyzed. Using the data recorded in specific areas extracted from the sagittal section in Figure 5B, representative spectra were obtained for white and gray matter. The spectra were filtered before being imported into Histomass, deleting peaks with intensities lower than 5% of the most intense peak (Figure S-2, SI). A complete identification of all the species in the spectra is not possible, due to the large abundance of peaks and the accuracy achieved in the tissues. Nevertheless, and despite the fact that many lipid species show a similar relative abundance in both types of matter, there are substantial differences in the relative abundance of GPCho species (i.e., 32:0; 36:1; 34:1) and SPM 36:0 (Figure S-2, SI).

CONCLUSIONS

In this study, we have explored different matrixes and experimental conditions to improve and extend the mass spectrometry-based lipids analysis methodologies. Of the different matrixes tested for MALDI-TOF, MBT offers at the same time a good S/N ratio and long acquisition times, allowing the recording of mass spectra from lipid extracts and directly from tissues.

Reproducibly accurate mass measurement in the 500−1800 Da mass range is demonstrated, allowing the identification of a large number of species, most of them belonging to the glycerolipid and sphingolipid families. It was possible to identify up to 37 different species on liver samples in positive (Table 1) and 32 species in negative ion mode (Table S-1, SI), while 43 species were detected in positive (Table 2) and 16 in negative mode in cerebral cortex samples (Table S-2, SI). As stated before, the major drawback of MBT is the large fragmentation pattern below ~500 Da. Such a difficulty has been partly overcome with the employment of Cs. By adding CsCl to the sample, it is possible to form the lipids Cs adducts, shifting the peaks 132 Da to higher masses. The low acidity of the matrix employed also allows the use of negative mode detection, which results in the identification of additional species, mainly GPIns and ST, whose detection in positive mode is hampered by the high intensity of GPCho signals.

Comparison with previous publications on MALDI-TOF detection of lipids[18,19,32−36] shows an ample agreement on the species detected for rat brain samples. Most of the previously detected species are also reported in this work. It is worthy of mention that several DAG and TAG species that are detected herein had not been previously identified. As seen from the references offered in Table 2 (and Table S-2, SI), the use of different matrixes usually results in the detection of different lipid species. To our knowledge, MBT enables the detection of the largest number of lipids in liver and brain samples both in extracted material and in situ, directly on tissue slices.

(36) Woods, A. S.; Jackson, S. N *AAPS J.* **2006**, *8*, E391–E395.

Abbreviations: DAG, diacylglycerols; DHA, 2,5-dihydroxyacetophenone; DHB, 2,5-dihydroxybenzoic acid; GPCho, glycerophosphocholines; GPEtn, glycerophosphoethanolamines; GPGro, glycerophosphoglycerols; GPIns, glycerophosphoinositols; GPSer, glycerophosphoserines; IMS, imaging mass spectrometry; MALDI, matrix-assisted laser desorption/ionization; MBT, 2-mercaptobenzothiazole; PNA, 4-paranitroaniline; SPM, sphingomyelins; ST, sulfatides; TAG, triacylglycerols; TOFMS, time-of-flight mass spectrometry.

ACKNOWLEDGMENT

This study was supported by the Spanish Ministry of Education and Science (SAF2007-60211) and the Basque Government (PE06UN24 and IT-325-07) to B.O. and O.F., SAIOTEK SAI07/46, Biscay County Council (DIPE07/05), Carlos III Health Institute (FIS PI070628), and UPV/EHU GIU07/50. L.L. and G.B.-G. are recipients of UPV/EHU predoctoral and postdoctoral fellowships, respectively. We thank Miss Adèle Hopley for critical and careful reading of the manuscript.

SUPPORTING INFORMATION AVAILABLE

Additional information as noted in text. This material is available free of charge via the Internet at http://pubs.acs.org.

Received for review August 7, 2008. Accepted October 6, 2008.

AC801662N